Paterson, H. F., Self, A. J., Garrett, M. D., Just, I., Aktories, K., and Hall, A. (1990). Microinjection of recombinant p21rho induces rapid changes in cell morphology. *J. Cell Biol.* **111,** 1001–1007.

Sahai, E., Alberts, A. S., and Treisman, R. (1998). RhoA effector mutants reveal distinct effector pathways for cytoskeletal reorganization, SRF activation and transformation. *EMBO J.* **17,** 1350–1361.

Sahai, E., and Marshall, C. J. (2002). ROCK and Dia have opposing effects on adherens junctions downstream of Rho. *Nat. Cell Biol.* **4,** 408–415.

Sahai, E., and Marshall, C. J. (2003). Differing modes of tumour cell invasion have distinct requirements for Rho/ROCK signalling and extracellular proteolysis. *Nat. Cell Biol.* **5,** 711–719.

Sahai, E., Olson, M. F., and Marshall, C. J. (2001). Cross-talk between Ras and Rho signalling pathways in transformation favours proliferation and increased motility. *EMBO J.* **20,** 755–766.

Sauzeau, V., Le Mellionnec, E., Bertoglio, J., Scalbert, E., Pacaud, P., and Loirand, G. (2001). Human urotensin II-induced contraction and arterial smooth muscle cell proliferation are mediated by RhoA and Rho-kinase. *Circ. Res.* **88,** 1102–1104.

Sebbagh, M., Renvoize, C., Hamelin, J., Riche, N., Bertoglio, J., and Breard, J. (2001). Caspase-3-mediated cleavage of ROCK I induces MLC phosphorylation and apoptotic membrane blebbing. *Nat. Cell Biol.* **3,** 346–352.

Vial, E., Sahai, E., and Marshall, C. J. (2003). ERK-MAPK signaling coordinately regulates activity of Rac1 and RhoA for tumor cell motility. *Cancer Cell* **4,** 67–79.

Vocero-Akbani, A., Lissy, N. A., and Dowdy, S. F. (2000). Transduction of full-length Tat fusion proteins directly into mammalian cells: Analysis of T cell receptor activation-induced cell death. *Methods Enzymol.* **322,** 508–521.

Wadia, J. S., and Dowdy, S. F. (2005). Transmembrane delivery of protein and peptide drugs by TAT-mediated transduction in the treatment of cancer. *Adv. Drug Deliv. Rev.* **57,** 579–596.

Wadia, J. S., Stan, R. V., and Dowdy, S. F. (2004). Transducible TAT-HA fusogenic peptide enhances escape of TAT-fusion proteins after lipid raft macropinocytosis. *Nat. Med.* **10,** 310–315.

# [12] Imaging and Photobleach Correction of Mero-CBD, Sensor of Endogenous Cdc42 Activation

*By* LOUIS HODGSON, PERIHAN NALBANT, FEIMO SHEN, and KLAUS HAHN

## Abstract

This chapter details quantitative imaging of the Mero-CBD biosensor, which reports activation of endogenous Cdc42 in living cells. The procedures described are appropriate for imaging any biosensor that uses two different fluorophores on a single molecule, including FRET biosensors. Of particular interest is an algorithm to correct for fluorophore photobleaching, useful when quantitating activity changes over time. Specific topics

METHODS IN ENZYMOLOGY, VOL. 406 0076-6879/06 $35.00
Copyright 2006, Elsevier Inc. All rights reserved.
DOI: 10.1016/S0076-6879(06)06012-5

include procedures and caveats in production of the Mero-CBD sensor, image acquisition, motion artifacts, shading correction, background subtraction, registration, and ratio imaging.

## Introduction

We recently described a novel biosensor to visualize and quantify Cdc42 nucleotide state in living cells (Nalbant *et al*., 2004). This biosensor (Mero-CBD) is based on a fragment of Wiskott–Aldrich syndrome protein (CBD, the Cdc42 binding domain) that binds only to activated GTP-bound Cdc42. The fragment is covalently labeled with a merocyanine dye whose fluorescence responds to the polarity of its solvent environment (Toutchkine *et al*., 2003). When the biosensor encounters and binds to activated Cdc42, dye fluorescence greatly increases. We use a GFP fusion of the WASP domain to enable ratio imaging; the ratio of dye/GFP fluorescence provides a quantitative readout of Cdc42 activation level. This approach is advantageous in that it monitors the activation of endogenous, untagged Cdc42. It provides a very bright signal resulting from direct excitation of a dye, enabling many time points to be monitored using low biosensor concentrations. This review first briefly expands on the published protocol for Mero-CBD preparation (Nalbant *et al*., 2004) but focuses primarily on a general procedure for quantitative imaging of Mero-CBD, including corrections for photobleaching and caveats in image-processing steps. These procedures will also be useful for other biosensors, including those based on FRET, which incorporate two different fluorophores. Of special interest is an algorithm to correct for photobleaching. We illustrate software operations with Metamorph, but the procedures are available in most commercial image processing packages.

## Mero-CBD Preparation

To avoid pitfalls that have been encountered by laboratories attempting to follow the published procedure for Mero-CBD production, the following notes are included:

1. It is important to use bacteria strain BL21(DE3) (Stratagene). Most problems encountered with producing the sensor have resulted from attempts to use similar strains (i.e., do not use BL21(DE3)pLysS). The protein should be induced and expressed at room temperature (26°) to increase the proportion of correctly folded, soluble CBD-EGFP.
2. Use Talon resin ($Co^{2+}$ affinity, Clontech Inc.) rather than Ni-NTA resin. Use 2 ml Talon resin (dry volume) for 3 g of cell pellet.

3. Use the suggested buffers. Apparently, unimportant modifications here have also caused problems in several cases.

4. Be sure to use enough buffer during lysis (i.e., for 3-g cell pellet use 35 ml total lysis buffer). CBD-EGFP needs to be in 50 m*M* $NaH_2PO_4$ buffer, pH 7.5, at a protein concentration of 100 $\mu M$. The reactive dye cannot be kept as a DMSO solution for more than 12 h. The dye/protein ratio in the reaction mixture should be 5:1 or 6:1.

5. When labeling, the reaction time is critical. Because EGFP contains internal cysteines, longer reaction times result in overlabeling and loss of EGFP signals. Optimize reaction times to produce a final dye/protein ratio of 0.7–0.9 in the purified product (starting point for optimization: 1 h at room temperature). Dye/protein is measured as described elsewhere (Nalbant *et al.*, 2004). The final Mero-CBD concentration after gel filtration is usually 50–60 $\mu M$.

## Cell Injection and Image Acquisition

Cells are microinjected on coverslips and allowed to recover for 30 min in an incubator before imaging. Mero-CBD can form puncta in some cells in about 3 h, possibly because of autophagocytosis, so timing these steps is important. During image acquisition, a dye image and a GFP image must be obtained at each time point for later dye/GFP division to obtain the final ratio image. It is important to show that localized activation is not an artifact caused by motion of the cell between acquisitions of the two images. For example, retraction of the edge can lead portions of an image to be divided by regions containing no cell. This will produce what seems to be very high activity at the cell edge. To control for motion artifacts, the order in which the images are taken can be reversed. Alternately, an EGFP picture can be taken both at the beginning and end of each sequence. Division of the earlier EGFP by the later EGFP image will reveal regions where movement has occurred (Fig. 1).

In our experiments, images are acquired at 30 sec–1 min time intervals using 2 by 2 binning on a full-field 1.3 k by 1.0 k CCD camera. The excitation light from a 100 W Hg arc lamp is too bright, necessitating use of neutral density filters. These are valuable also to decrease bleaching. Bleaching is much less for samples exposed over longer time to weak illumination, rather than briefly to bright light, even when the total light exposure is the same. This is also beneficial to cell health. We routinely use 25–36% transmittance (ND 1.4–1.0) neutral density filters. These numbers are provided only as a rough example, because exposure times will depend on the quantum efficiency and noise characteristics of the

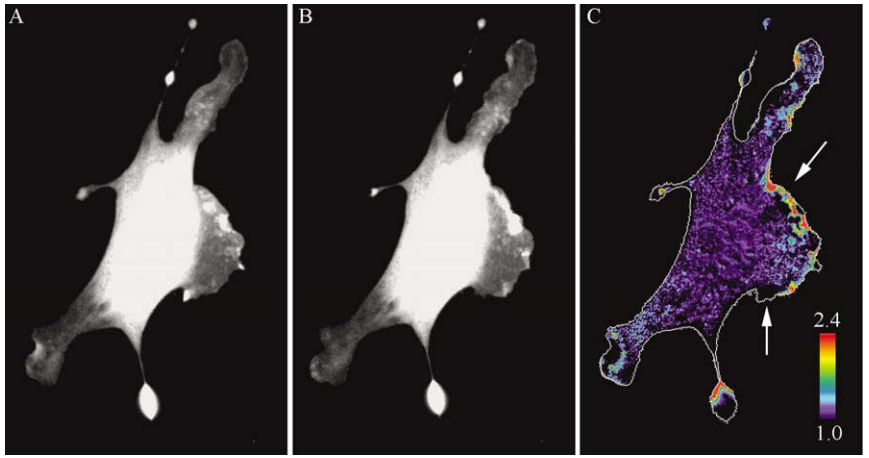


FIG. 1. Effects of motion artifacts on ratiometric measurements. (A and B) EGFP images taken before and after I-SO acquisition. Dividing the second EGFP image by the first shows where motion has occurred during the acquisition sequence. In this example, (B)—second EGFP acquisition—was divided by (A)—first EGFP acquisition—to produce ratiometric (C). Areas that underwent protrusion generated artificial high ratios (upper white arrow) and low ratios (lower white arrow). The outline of the cell is shown in white in (C).

camera. Twelve-bit cameras have an intensity range of 0–4096; to obtain sufficient dynamic range, we target roughly 1500–3000 as the maximum pixel value in the field of view. We carefully monitor the pixel intensities near the cell periphery where the signals are usually low, to be at least 100–150 over background values.

In Mero-CBD, we used two fluorophores with very different wavelengths to minimize bleed through of one fluorescence channel into the other. Even with lenses well corrected for chromatic aberration, switching between two such very different wavelengths necessitates moving the objective to maintain the same focal plane. In our system, the objective must be moved approximately 200 nm. We determine the appropriate offset in control experiments using commercially available beads that fluoresce over a wide range of wavelengths (Molecular Probest, Eugene Oregon).

## Bandpass Filters and Dichroic Selection

Motion-induced artifacts in activity levels can be eliminated by taking the two images simultaneously, either using two cameras or a device that obtains two images on different portions of the same CCD chip (hardware for both is commercially available). Either approach requires

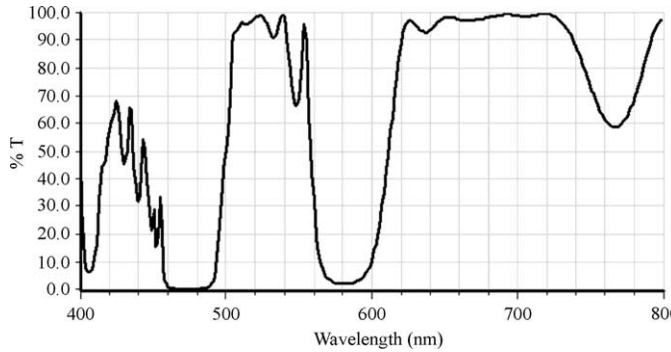


FIG. 2. Transmittance spectra of the custom multiband pass dichroic mirror designed by Chroma Technology for simultaneous imaging of I-SO and EGFP.

use of appropriate dichroic mirrors to send different wavelengths to the two images; such dichroics and matching excitation and emission filters have been designed for Mero-CBD by the Chroma Company (Chroma Technology, Rockingham, VT) (Fig. 2; bandpass filters = HQ470/40, HQ525/50 for EGFP, and HQ580/30, HQ630/40 for I-SO). Because the I-SO dye and EGFP have different brightness, the relative amounts of excitation light at each wavelength must be controlled by the filters if images are to be obtained simultaneously. Dyes are being developed that can be excited by two different laser lines. This will simplify adjustment of excitation intensities.

One of the key concerns with biosensors using two fluorescent components is the bleed through of emission from one fluorophore into the image of the other. When both fluorophores are on the same molecule, this is not so critical, because the two fluorophores are equally distributed throughout the cell. In such cases, bleed through affects the linearity of response to physiological stimuli, but this has been ignored in most experiments, where it is considered an acceptable error. When the two fluorophores are on separate molecules, it is essential to correct for bleed through; otherwise, differences in subcellular distribution of the two fluorophores can profoundly affect results. This has been covered in detail elsewhere (Chamberlain and Hahn, 2000; Chamberlain *et al.*, 2000).

## Shading Correction

The first step of image analysis is to correct for uneven illumination across the field of view. This is present in almost all images, including those taken with Plan-corrected objectives, but can be greatly reduced using

fiberoptic light scramblers. Users can check their images by taking a diagonal line-scan of an empty field. To correct for shading, obtain images without any sample present, using the integration times and illumination conditions applied to actual samples. This should be part of each experiment, using either cell-free areas within the coverslip or mounting a fresh coverslip with identical media. In the latter case, it is easier to focus if a mark is made on the side of the coverslip where the cells would have been. Usually, 20–30 shading images are acquired and averaged to produce a single shade correction image for each fluorescence channel. This averaging reduces stochastic camera noise associated with image acquisition (Fig. 3). Once the averaged shading images are acquired, shading correction is simply a matter of dividing the sample image by the shading image. Here, care must be taken to prevent floating point errors. Because many common software programs do not use a ''floating'' decimal place in specifying pixel intensities, there are effectively rounding-off errors in the calculations. Metamorph, which does have this problem, offers a convenient plug-in module for shade correction; images are multiplied by a scaling factor to increase pixel intensity values before division, thus effectively eliminating these errors. One either scales so that the maximum pixel value in the image remains on scale or simply specifies a number high enough to eliminate the error (i.e., 1000 for 12-bit images acquired as

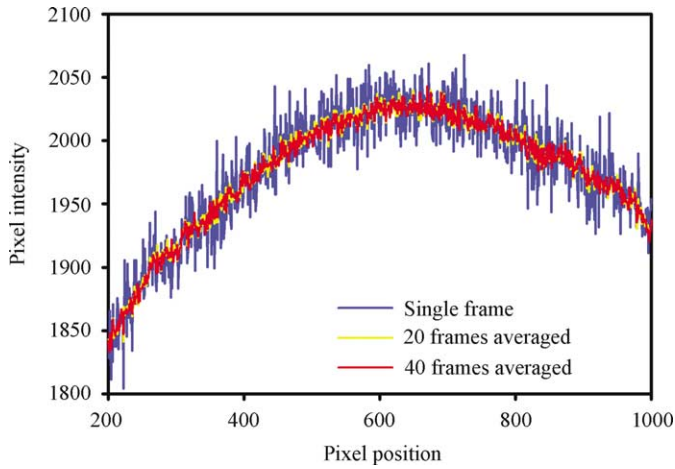


FIG. 3. The effect of averaging on shading correction images. A sample-free field of view was imaged under identical illumination conditions once (blue), 20 times (yellow), and 40 times (red) and averaged. Averaging of many frames reduces the stochastic noise in the image.

described previously). The same scaling factor should be specified for both fluorescence images before division, so that final ratios are not affected; this is important when a set of final images are to be compared with one another, as in a time course. Matlab (Mathworks, Natick, MA) codes can be written to process images using floating-point procedures.

### Background Subtraction

Because of shade correction, cell-free areas within the image show uniform intensity. Background subtraction can, therefore, be accomplished by choosing a small area within the cell-free background and subtracting the average intensity from the entire image. It is important to choose the same background region in all image pairs to minimize artifacts. Metamorph offers a convenient plug-in module (''Use region as background'') to expedite this; one selects a background region in the first fluorescence image of the ratio pair, which can then be pasted onto the second fluorescence image. When using such a utility for an entire series of images, it is important that the average background from the first image pair not be used for the entire image stack. The same background region can be applied to each image, but average background must be determined and subtracted anew for each time point in the image stack.

### Image Registration

For ratiometric sensors, one image is divided by another to obtain the final map of protein activity distribution (i.e., for Mero-CBD, I-SO image divided by EGFP to obtain Cdc42 activation). One of the most challenging aspects of this procedure is properly registering the two images before division. It is very difficult to change the microscope so that pixel misalignment does not occur, because it stems from so many causes (varying thickness and alignment of dichroics and filters; movement of many microscope components including filter wheels, turrets, and stages; temperature fluctuations; ambient vibrations; chromatic aberration within the objective lens). Figure 4 illustrates the effects of misalignment on ratiometric analysis. These include characteristic artifacts that warn of misalignment: ''edge artifacts'' where ratio values are high on one side of the cell and low on the opposite side, and bright shading on one side of objects within the cell such as the nucleus. Automated methods for image registration are available (Shen *et al.*, 2004), but manual methods can be used successfully and remain more accurate in some cases. A Metamorph ''Color align'' plug-in module can be used to determine the relative pixel shifts of up to three fluorescence channels. One fluorescence image channel is held stationary, whereas the other is shifted manually while following the overlay of red and

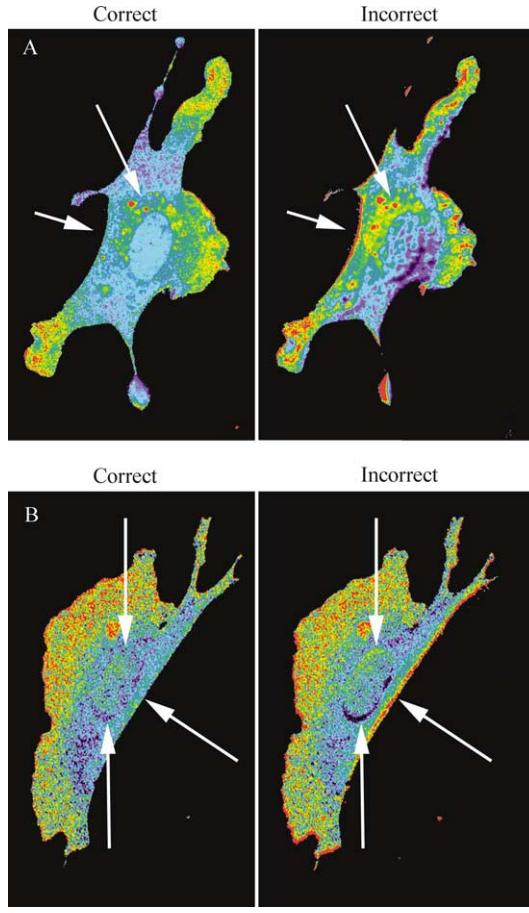


FIG. 4. Image registration artifacts. (A) Example of misregistration producing artifactual edge effects and spurious intracellular features (white arrows). The images were misaligned by 5 whole pixels in both the x and y directions. (B) More subtle effects of misalignment resulting in edge effects around the nucleus (white arrows) plus an acute, high ratio region at the cell edge. In this case, the shifts were less than 1 pixel (0.1 pixel in the x direction, −0.8 pixel in the y direction). A telltale sign of misalignment is high values on one side of the misaligned object and low values on the opposite side.

green pseudocolor images. The resulting x and y pixel shift values can be applied to other images from the same experiment using the ''Subpixel shift'' module, which can make corrections at subpixel accuracy. If using two cameras, rotational alignment must be performed before image acquisition (a grid-type micrometer can be used). This is critical, because

rotational correction is much more difficult to perform computationally. Off-line methods to correct for such issues are available (Danuser, 1999).

### Image Masking

Dividing two images will introduce noise and hot spots wherever the intensity in the either image is too low to use. Division of small numbers can greatly distort variations from pixel to pixel. Although intensities within sufficiently bright portions of the image may be well over 100, values can be below 10 in the background or dim portions of the cell. This produces large fluctuations even though the actual difference in brightness between neighboring pixels is small (compare 5/1 versus 1/5). To limit ratio calculations to image regions with sufficient intensity, various masking operations are used. The simplest is to set areas outside of the cell to zero by manually drawing an outline of the cell edge. Alternately, masking can be based on exclusion of pixels below a user-specified minimum intensity level. Masking can be based on volumetric markers such as fluorescent dextrans or membrane markers to unambiguously specify the true cell boundary. In the case of Mero-CBD, distribution of the biosensor is sufficiently close to the cell edge to use biosensor signaling in defining the cell boundaries. To produce the mask of the cell edge, the fluorescence image of the brighter signal (EGFP) is thresholded by histogram intermodal localization. This is a straightforward process (''Threshold Image'' command in Metamorph). After proper shading correction and background subtraction, the intensity versus pixel number histogram usually will show a large distinct peak for low intensity pixels and a spread of high intensity pixels comprising the image (Fig. 5). The low-end threshold value is determined by trial and error. The upper bound needs to be set at the maximum possible value for the image (65,535 for a 16-bit image). When processing a series of images in a stack, such as from a time-lapse experiment, it is important to compare the low-end threshold value selected for the first and last images. The photobleaching of biosensor will shift the low end of the intensity distribution histogram downward over time. Therefore, using a threshold based on the first image would eliminate important areas in cells from later time points. Threshold values are usually determined for later time points. A mask can be produced based on the selected thresholds.

In Metamorph, the ''Clip'' tab within the ''Threshold Image'' module is used to produce a binary mask in 16 bit. This will produce a binary mask, where regions outside the selected area are uniformly zero, whereas inside is 65,535. The ''Arithmetic'' function is then used to divide the binary mask by a constant (65,535) to produce a true binary mask containing the pixel value of one inside the masked region and zero outside. This binary mask is

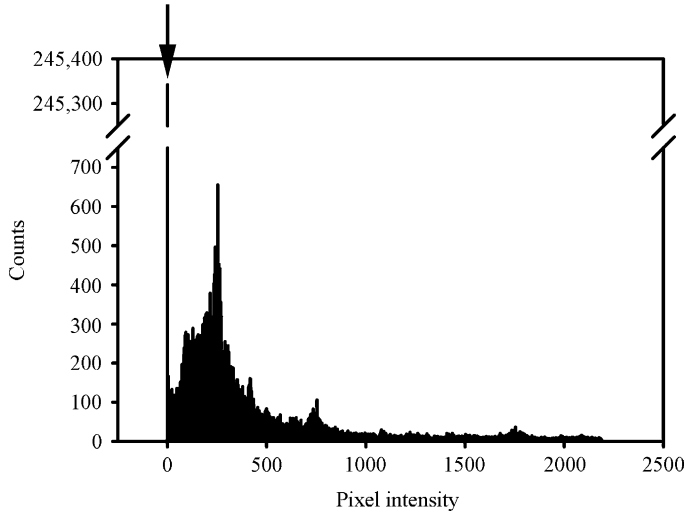


FIG. 5. A representative histogram from a shading corrected, background subtracted image. The prominent histogram spike at zero intensity (arrow) is followed by a continuous distribution of non-zero intensity peaks.

multiplied by the fluorescence images before ratio calculation. It is important that the color scheme used for image display uses a specific color, usually black, for pixels in which the numerator or denominator is set at zero.

## Ratio Calculation

As with shading correction, floating point errors must be considered during the final division that produces the ratio image (see preceding). In the Metamorph "Arithmetic" module, a scaling factor of 1000 is specified as a multiplication factor during the ratio calculation. Smaller factors (10–100) tend to produce a stepped histogram distribution (Fig. 6). The same scaling factor needs to be applied for each ratio calculation if quantitative comparison of ratio images is desired. The pseudocolor display of the ratio image is scaled to emphasize or study certain intensity ranges, bringing out different features in the image. An image without the accompanying pseudocolor scale is almost meaningless.

## Photobleach Correction

Time-lapse imaging of fluorescence is complicated by photobleaching of the biosensor. Real activation changes are superimposed on a steady decrease in fluorescence intensity, at different rates for each fluorophore in the sensor. There is too much variability to determine a standard bleaching

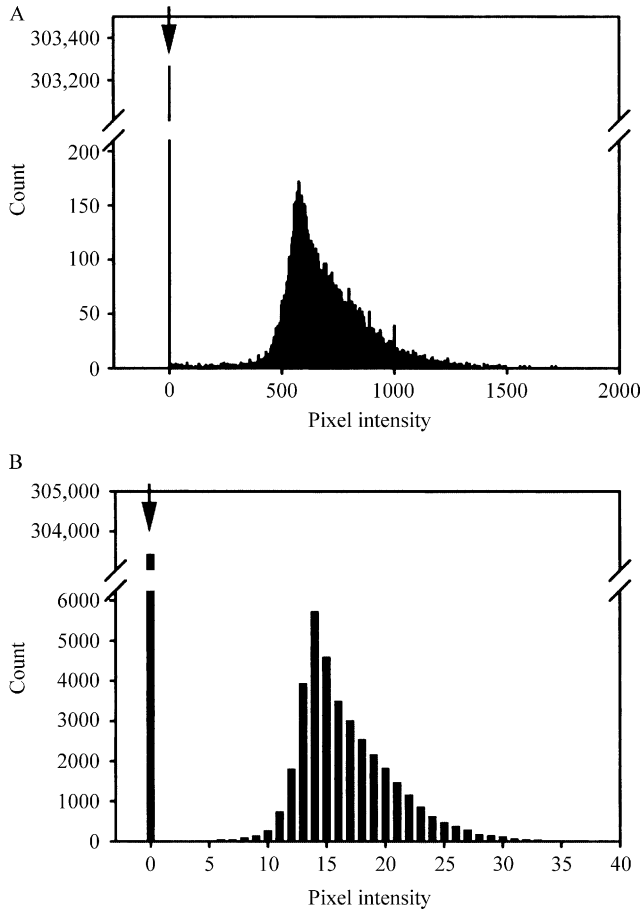


FIG. 6. Effect of multiplication factor during ratiometric calculation. In software that does not use floating point operations, ratiometric division requires a scaling factor. (A) A smoothly varying histogram distribution of a ratio image produced using a scaling factor of 1000. (B) The same ratio image with a scaling factor of 25. Although the general trend of the data is similar, the histogram in (A) retains higher resolution and produces a smoother ratio image. In both panels, background value of zero is marked with an arrow.

curve in separate control experiments. In real experiments, fitting curves to the data is complicated by the fact that bleaching is superimposed on the fluorescence changes the biosensor was designed to undergo.

Photobleach correction for Rho family sensors is simplified by the fact that only ~5% of GTPases are active (Del Pozo *et al.*, 2002; Ren *et al.*, 1999), and that even this ~5% is localized to specific regions (i.e., cell periphery, membrane ruffles). We can assume that averaging all the

low-activity regions in the cell provides a reasonable approximation of the intensity of biosensor in the inactive state. Even if we include all the activated material, the average for Mero-CBD would be too high by only 10% (Mero-CBD shows a 3× change in I-SO intensity between the active and inactive state. Therefore, the whole cell average would be at most $5(3) + 95(1)/100 = 1.1$. Using only the portions of the cell where there is minimal, activated Cdc42 should reduce this error greatly.

To determine the bleaching kinetics, changes in I-SO and EGFP intensities were measured. Intensities can be measured using the masked fluorescence images, because the background is at or near zero and can be readily removed from the calculations. A Metamorph journal can be constructed to automate these procedures after the initial determination of the intensity threshold values from the EGFP and I-SO image stacks. Background subtraction removes any signal from dye and fluorophores outside the cell, which may bleach differently in the extracellular environment.

Because relatively little change in ratio occurs near the cell nucleus, and the thick nuclear regions are brighter than the cell periphery, it is straightforward to set a threshold value that includes only the regions near the nucleus. This is better than using the Region tool to select a small area within the nucleus for measurement, because such measurements would be skewed by cell movement.

The average intensity values determined for EGFP and I-SO at each time point are normalized; each is divided by the initial value ($t = 0$ time point) to produce a normalized ratio change as a function of time. This curve takes the form of an exponential decay function (Patterson and Piston, 2000) and is fitted to a double exponential function:

$$y = A \cdot e^{-B\times} + C \cdot e^{-D\times} \tag{1}$$

Curve fitting provides a robust and objective means to produce a bleach correction function. For example, if a physiological stimulus produces a large, transient change in ratio values, it is possible to analyze only portions of the curve before stimulation and after effects of stimulation have subsided. When provided with a segment at the beginning of the curve and a few ratio values near the end of the assay, the double exponential function can approximate the general trend of the photobleach curve. Once the photobleaching function is determined, it can be used to obtain a function for correcting the data: a simple inverse of the photobleach function. For convenient application to Metamorph ratio image stacks, a simple Matlab program has been provided (Appendix A). A version with graphical user interface can be downloaded from http://www.med.unc.edu/pharm. The program reads consecutively numbered image files in tiff format, reads an

MS-Excel data sheet containing the raw intensity values of the I-SO and EGFP channels, calculates the photobleach correcting function, and applies this to the original images to output the corrected and consecutively numbered tiff images.

## Conclusion

We hope that this description of image-processing procedures, including common pitfalls, will be valuable for those wishing to use the many biosensors that require ratio imaging of two separate fluorophores. In the future, ratiometric sensors of protein activity that are based on shifts in the fluorescence maxima of a single dye should further simplify ratio imaging, eliminating altogether the need for bleaching corrections and enabling precise quantification without bleed through correction.

## Appendix A

```
%%%
```

```
Dname = input('Enter Excel file name for the intensities, Plane#/ Num/Denom; without Excel file extensions: ','s'); % This sets file name for intensities
DNAMEIN = sprintf ('%s.xls', dname);
data_all = xlsread(DNAMEIN);
Plane_initial = data_all(1:I);  % Plane array goes from 1 to I
num_Int = data_all(I+1:2*I);  % absolute value intensities for the numerator
denom_Int = data_all(2*I+1:3*I);  % absolute value intensities for the denominator
num_Int_norm = num_Int ./ num_Int(1);  % calculates normalized intensity values for numerator, normalized to t = 0
denom_Int_norm = denom_Int/denom_Int(1);  % calculates normalized intensity values for denominator, normalized to t = 0
Plane = (Plane_initial - 1).';  % makes plane array start from zero instead of 1 for data fitting purposes
Ratio = (num_Int_norm/denom_Int_norm).';  % calculates the ratio of the normalized intensities
outliers = ~excludedata (Plane, Ratio, 'range', [0 0.1]); % sets fit exclusion range in Y values [fresult,gof] = fit(Plane, Ratio, 'exp2', 'exclude', outliers); % double exponential fit, Plane numbers as X and normalized Ratio as Y
display (fresult);  % displays fitted parameters and coefficients
display (gof);  % displays goodness of fit parameters
Fit_ratio = fresult(Plane); % producing fitted curve using the plane numbers
CF = 1/Fit_ratio;  % correction factor is 1 over the ratio decay function
a = num2str(fresult.a); b = num2str(fresult.b); c = num2str(fresult.c); d = num2str(fresult.d); rsq = num2str(gof.rsquare);
coef = sprintf('a = %s ; b = %s', a, b);
coef2 = sprintf('c = %s ; d = %s', c, d);
coef3 = sprintf('r^2 = %s', rsq);
plot(Plane, Ratio, 'rd', Plane, fresult(0:I-1), 'b-'); % Plots results
title('Double exponential fit to Photobleach data');
xlabel('Plane Number');
ylabel('Normalized Ratio Decay');
legend('Data', 'Fit');
axis([0, I, 0, 1.2]);
text (2, 0.4, 'y = a exp(b*x) + c exp(d*x)');
text (2, 0.33, coef);
text (2, 0.26, coef2);
```

```
text (2, 0.19, coef3);
% Writes data files for output and plotting off-line
fid = fopen('Fit_Decay_curve.txt', 'a');
fprintf(fid, '%12.6f \r', Fit_ratio);
fclose(fid);
fid = fopen('Actual_Ratio_data.txt', 'a');
fprintf(fid, '%12.6f \r', Ratio);
fclose(fid);
fid = fopen('goodness_of_fit.txt', 'a');
fprintf(fid, '%12.6f \r', gof);
fclose(fid);
% Image processing starting at this point, using the CF as the correction
if I < 100;
if I < 10;
for mult_rep = 1:I;
counter = mult_rep;
FNAMEIN = sprintf('%s%i.tif', fname, counter);
ratio = imread(FNAMEIN, 'tif');
R = double(ratio);
CR = R .* CF(counter); %Array element by element multiplication
CR_out = uint16(CR);
FNAMEOUT = sprintf('out_%i.tif',counter);
imwrite(CR_out, FNAMEOUT, 'tif', 'compression', 'none'); % write
  output file
end;
else;
for mult_rep = 1:I;
counter = mult_rep;
if counter < 10;
FNAMEIN = sprintf('%s0%i.tif', fname, counter);
else;
FNAMEIN = sprintf('%s%i.tif', fname, counter);
end;
ratio = imread(FNAMEIN, 'tif');
R=double(ratio);
CR = R .* CF(counter); %Array element by element multiplication
CR_out = uint16(CR);
if counter < 10; FNAMEOUT = sprintf('out_0%i.tif',counter);
else;
FNAMEOUT = sprintf('out_%i.tif',counter);
end;
```

```
imwrite(CR_out, FNAMEOUT, 'tif', 'compression', 'none'); % write
  output file
end;
end;
elseif I > = 100;
for mult_rep = 1:I;
counter = mult_rep;
if counter < 10;
FNAMEIN = sprintf('%s00%i.tif', fname, counter);
ratio = imread(FNAMEIN, 'tif');
R = double(ratio);
CR = R .* CF(counter); %Array element by element multiplication
CR_out = uint16(CR);
FNAMEOUT = sprintf('out_00%i.tif',counter);
imwrite(CR_out, FNAMEOUT, 'tif', 'compression', 'none'); % write
  output file
elseif counter < 100;
FNAMEIN = sprintf('%s0%i.tif', fname, counter);
ratio = imread(FNAMEIN, 'tif');
R = double(ratio);
CR = R .* CF(counter); %Array element by element multiplication
CR_out = uint16(CR);
FNAMEOUT = sprintf('out_0%i.tif',counter);
imwrite(CR_out, FNAMEOUT, 'tif', 'compression', 'none'); % write
  output file
elseif counter > = 100;
FNAMEIN = sprintf('%s%i.tif', fname, counter);
ratio = imread(FNAMEIN, 'tif');
R = double(ratio);
CR = R .* CF(counter); %Array element by element multiplication
CR_out = uint16(CR);
FNAMEOUT = sprintf('out_%i.tif',counter);
imwrite(CR_out, FNAMEOUT, 'tif', 'compression', 'none'); % write
  output file
end;
end;
end;
```

## Acknowledgment

This work was supported by The National Institutes of Health (GM057464 and GM064346).

## References

Chamberlain, C., and Hahn, K. M. (2000). Watching proteins in the wild: Fluorescence methods to study protein dynamics in living cells. *Traffic* **1,** 755–762.

Chamberlain, C. E., Kraynov, V., and Hahn, K. M. (2000). Imaging spatiotemporal dynamics of Rac activation *in vivo* with FLAIR. *Methods Enzymol.* **325,** 389–400.

Danuser, G. (1999). Photogrammetric calibration of a stereo light microscope. *J. Microscopy* **193,** 62–83.

Del Pozo, M. A., Kiosses, W. B., Alderson, N. B., Meller, N., Hahn, K. M., and Schwartz, M. A. (2002). Integrins regulate GTP-Rac localized effector interactions through dissociation of Rho-GDI. *Nat. Cell Biol.* **4,** 232–239.

Nalbant, P., Hodgson, L., Kraynov, V., Toutchkine, A., and Hahn, K. M. (2004). Activation of endogenous Cdc42 visualized in living cells. *Science* **305,** 1615–1619.

Patterson, G. H., and Piston, D. W. (2000). Photobleaching in two-photon excitation microscopy. *Biophys. J.* **78,** 2159–2162.

Ren, X. D., Kiosses, W. B., and Schwartz, M. A. (1999). Regulation of the small GTP-binding protein Rho by cell adhesion and the cytoskeleton. *EMBO J.* **18,** 578–585.

Shen, F., Hodgson, L., Rabinovich, A., Pertz, O., Hahn, K. M., and Price, J. H. (2004). Functional proteometrics for cell migration. *Cytometry.* In press.

Toutchkine, A., Kraynov, V., and Hahn, K. (2003). Solvent-sensitive dyes to report protein conformational changes in living cells. *J. Am. Chem. Soc.* **125,** 4132–4145.

# [13] Cdc42 and PI(4,5)$P_2$-Induced Actin Assembly in *Xenopus* Egg Extracts

*By* ANDRES M. LEBENSOHN, LE MA, HSIN-YI HENRY HO, and MARC W. KIRSCHNER

## Abstract

*Xenopus* egg cytoplasmic extracts have been used to study a variety of complex cellular processes. Given their amenability to biochemical manipulation and physiological balance of regulatory proteins, these extracts are an ideal system to dissect signal transduction pathways leading to actin assembly. We have developed methods to study Cdc42 and PI(4,5)$P_2$-induced actin assembly in *Xenopus* egg extracts. In this chapter, we describe detailed procedures to prepare *Xenopus* egg extracts, Cdc42, and PI(4,5)$P_2$ for use in actin assembly experiments. We also describe a fluorometric pyrene actin assay for quantitative kinetic analysis of actin polymerization and a microscopic rhodamine actin assay for quick measurement of actin rearrangements in extracts. Finally we provide a protocol for immunodepletion of proteins and discuss the use of immunodepletion

METHODS IN ENZYMOLOGY, VOL. 406 0076-6879/06 $35.00
Copyright 2006, Elsevier Inc. All rights reserved.
DOI: 10.1016/S0076-6879(06)06013-7